PAN
ARCHIVES OF ACOUSTICS
Vol. **46**, No. 1, pp. 3–15 (2021)
DOI: 10.24425/aoa.2021.136555

Review Paper

An Educational Overview of Ultrasound Probe Types and Their Fields of Application

Ramona DE LUCA[(1)]*, Leonardo FORZONI[(1)], Francesca GELLI [(1)], Jeffrey BAMBER[(2)]

[(1)] *Esaote S.p.A.*
Florence, 50127, Italy
*Corresponding Author e-mail: ramona.deluca@esaote.com

[(2)] *Institute of Cancer Research and Royal Marsden NHS Foundation Trust*
London, SM2 5NG, United Kingdom

(*received May 29, 2020; accepted November 25, 2020*)

The ultrasound (US) imaging market is fast-changing in terms of needs, trends and tendencies as it undergoes rapid innovations. Due to technological improvements, a variety of US probe types is available to cover a wide range of clinical applications. The aim of this paper is to provide information to healthcare professionals to select the appropriate probe for the intended use and the desired performance/price ratio. This work describes the majority of conventional, special and unique US probe types currently available on the market, together with technological insights that are responsible for image quality and a list of some of their clinical applications. The description of the inner transducer technologies allows to understand what contributes to different prices, features, quality level and breadth of applications. The comparison of current US probes and the analysis of advanced performances arising from the latest innovations, may help physicians, biomedical and clinical engineers, sonographers and other stakeholders with purchasing and maintenance commitments, enabling them to select the appropriate probe according to their clinical and economical needs.

Keywords: ultrasound probes typology; technologies; clinical applications.

1. Introduction

Being sufficiently non-hazardous, portable, compact, low-cost and real time, ultrasound (US) is the most widely used non-invasive diagnostic imaging modality worldwide (Azhari, 2012). Along with its ability to provide images of internal body anatomy, detect the dynamic movement of organs, and reveal details of blood flow in real time (Szabó, 2004), it offers a variety of imaging approaches, each providing a different type of clinical information. These techniques include contrast enhanced ultrasound, elastography, ultrasound computed tomography and molecular imaging (Azhari, 2012). Diagnostic US imaging is used for many parts of the body (e.g. abdomen, vascular, heart, musculoskeletal, women's health) (Andreoni *et al.*, 2015), on fetal, neonatal, pediatric, adult, human and animal patients, and by different users (e.g. sonographers, physicians, radiologists, surgeons, anesthesiologists, midwives, paramedics, and veterinarians). US systems consist of two main parts which are the console (including the keyboards, the mouse/trackball, the monitor and often a touch screen) and the probe that is optimized for specific clinical imaging applications. Classification of US machines is typically based on whether they are cart-based or portable, and on their position in the price/performance range (Premium, High-End, Mid-End, Low-End). US imaging systems undergo rapid technology progress, and this leads a quick rotation of products available on the market and rapid change of price/performance ratio. In this complex scenario, US probes have a significant impact upon both image quality and ergonomics. Ultrasonic probes are specialized to each intended use (i.e., region of interest, access window, and maximum scan depth) and recent designs enable more significant and consistent diagnostic information, faster and easier scanning and increased reliability, due to important technology improvements. The purpose of this paper is to provide an analysis of the types of US probes

that are currently on the market, giving insights into the latest technologies as well as clinical applications. The description of how the latest innovations influence both probe type and advanced performance may help in understanding of what contributes to different prices, features, quality level and breadth of applications. Therefore, this overview aims to help users and other stakeholders with purchasing and maintenance commitments, to select the appropriate probe according to their clinical and economic needs.

2. Ultrasonics

Ultrasonic transducers are devices that generate and receive US waves; they convert the electric energy into ultrasonic energy, and *vice-versa*. When either designing or selecting an US probe, technical parameters (such as central frequency, bandwidth, front matching layer, and backing material) and performance parameters (among others, field of view, spatial and contrast resolution) must be considered if the probe is to meet the intended use.

2.1. Basic principles of ultrasonic transducer design and construction

The ultrasonic transducer converts electrical pulses to ultrasonic waves that are sent to the body and are reflected or backscattered by internal anatomic structures. The transducer then detects the consequent echoes and converts them to electrical signals that the system processes and transforms into an image. Generally, it is made of an acoustic stack composed of a piezoelectric ceramic layer, a backing block, an acoustic matching layer and a lens (Szabó, 2004). Innovation on these materials is crucial for developing high-performance probes that will provide increasingly accurate and reliable images. Modern US transducers consist of an array of multiple small piezoelectric elements, each part of the acoustic stack (Fig. 1).

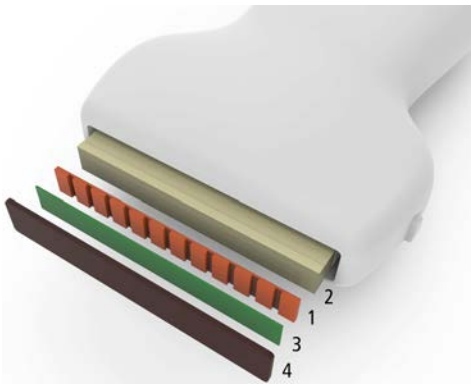

Fig. 1. Sketch of a typical medical ultrasound transducer based on an array with multiple small piezoelectric elements (1) attached to a matching layer (3), a backing layer (2) and an acoustic lens (4).

The piezoelectric layer is the active material that converts the electrical signal into an US wave and *vice-versa* (Yu *et al.*, 2009). The backing block, consisting of a heavy metal-based material (Kochański *et al.*, 2015) bonded on the back face of the piezoelectric elements, has acoustic impedance and absorption optimized to reduce reflections from the back face of the piezoelectric, in order to produce a pulse with less ringing. As a result, higher image resolution is provided. A matching layer, a typically loaded epoxy resin bonded on the front face of the piezo-elements, improves the transfer of energy to the tissues by compensating for the acoustic impedance mismatch between the stiff piezo-elements and soft biological tissues. This results in enhanced sensitivity. It also reduces reflections at the front face of the piezoelectric element of the ultrasonic waves that travel in the forward direction, acting like the backing layer to shorten the pulse, increasing the bandwidth and therefore to further improve image resolution. Significant contributions to the performance of modern probes arise from the application of multiple adaptive matching layers and backing layers that use the dematching layers (Chen, Wu, 2002). Multiple adaptive matching layers consist of different thin layers made of materials whose acoustic impedance changes gradually from layer to layer, from the impedance of the piezoelectric material to that of human tissues (Table 1). The tapered reduction of the impedance mismatch allows the transfer of as much energy as possible to the body and this results in deeper penetration. Enhanced resolution arises from shorter pulses, and improved harmonic-imaging performance from increased bandwidth and sensitivity.

Table 1. Example of acoustic impedance (Z) matching provided by multiple matching layers (Spicci, 2013), between the Z of the piezoelectric ceramic lead zirconate titanate (PZT) and that of soft biological tissues.

	Z (MRayl)
PZT	30
1st ML	14
2nd ML	8
3rd ML	3
4th ML	2
Soft biological tissues	1.5

Dematching layers, sandwiched between the backing block and the piezo-elements, reflect the energy transmitted backwards by the element and retransmit it forwards. This reuse of acoustic energy that would otherwise be dispersed, increases sensitivity and makes for less heat dissipation, preserving probe performance in terms of sensitivity and penetration. Manufacturers recognize the importance of the thermal management of US probes and show strong interest in developing new technologies to dissipate heat within the probe.

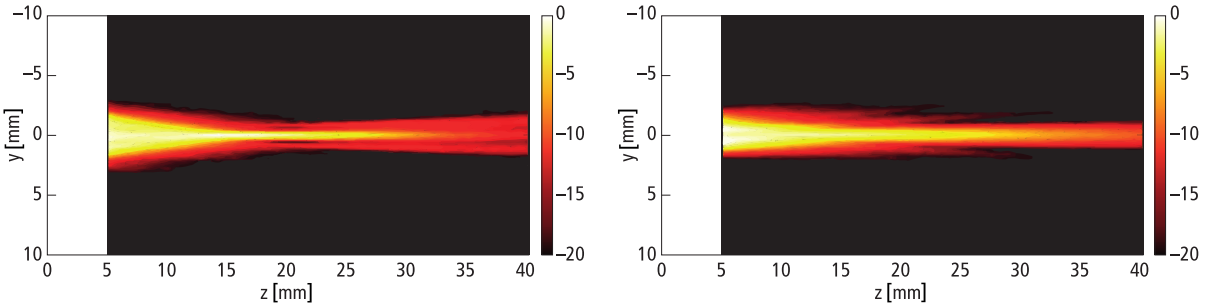

Fig. 2. Examples of beam pattern profile (dB relative to the last axial maximum, z is the propagation direction and y is the elevation direction). Depending on the region of interest, different elevation aperture size (element length) and focusing of the ultrasonic transducer are required to reach the desired scan depth and resolution.

Two examples of an efficient cooling system are: a heat transfer device made of a graphene-based material, either pure graphene or a graphene-loaded resin, which is placed on the front of the transducer assembly to work also as part of the matching layer into the body (Spicci *et al.*, 2017); a cooling system embedded at the rear of the transducer, composed of a heat spreader, which transfers heat away from the heat source, and a heat sink, which dissipates the heat (Cho *et al.*, 2012).

An acoustic lens is used to focus the US beam in the plane perpendicular to the imaging plane (Kochański *et al.*, 2015; Maione *et al.*, 1999) (Fig. 2). The lens layer typically consists of a material with acoustic impedance close to that of human tissues, low absorption, and high mechanical strength. In conjunction with specifically designed geometry, it provides an appropriate slice thickness that enables uniform sensitivity and good signal-to-noise ratio across the whole field of view (i.e. minimizing artefacts such as reverberations, increasing contrast resolution and improving border definition of anatomical structures) and high reliability.

To ensure electrical safety, further increase the robustness of US transducers and guarantee longer product life, an electrically-insulating and chemically-resistant layer (such as parylene (Zhou *et al.*, 2014)) is placed underneath the lens.

2.2. Piezoelectric materials for ultrasonic transducers

In the last decades, lead zirconate titanate (PZT) ceramic was the predominant piezoelectric material for building US transducers, due to its excellent piezoelectric properties, chemical inertness, physical strength, and easy and inexpensive manufacturing (Yue *et al.*, 2014). However, PZT has some drawbacks, such as a high acoustic impedance (20 times higher than human soft tissues) and power loss from low electromechanical conversion efficiency, which have led the need to the investigation of a new generation of piezoelectric materials, such as single crystal PMN-PT (lead magnesium niobate-lead titanate) and PIN-PMN-PT (lead indium niobate-lead magnesium niobate-lead titanate). PZT ceramic is made of a dense polycrystalline structure of random grains, while single crystal ceramic is grown in monocrystalline form. The behaviour of single crystal in an electric field is different from that of PZT ceramic: a single crystal shows dipoles almost aligned, while dipoles are more randomly arranged in PZT ceramic (Fig. 3).

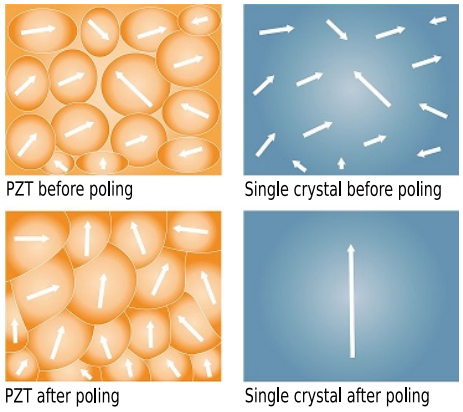

Fig. 3. The process of poling is applied to a piezoelectric material (i.e. it is exposed to a strong electric field) before using it. As a single crystal is grown in a monocrystalline form, while PZT ceramic is made of a dense polycrystalline structure of random grains, it exhibits an increased efficiency of poling: single crystal shows almost all dipoles aligned, while dipoles are more randomly arranged in a PZT ceramic. As a result, a single crystal has enhanced electro-mechanical properties compared to PZT, leading to improved imaging performance.

Therefore, single crystals exhibit an electromechanical coupling factor (k_{33}) and a piezoelectric coefficient (d_{33}) up to 90% and three times higher than PZT, respectively. Typically, lead-based single crystals have $d_{33} \sim 2000$ pC/N and $k_{33} \sim 0.9$ (Ming Lu, Proulx, 2005). As a consequence, compared to PZT, single crystals provide up to 20–25% wider bandwidth (Fig. 4), greater sensitivity, therefore lower loss and deeper penetration than PZT, enabling more detailed diagnostic information even for difficult-to-image patients (Yu *et al.*, 2009).

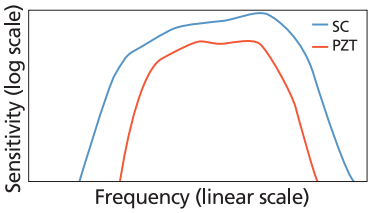

Fig. 4. Single crystal (SC) provides up to 20–25% wider bandwidth than PZT, with greater sensitivity and hence stronger penetration, allowing enhanced imaging quality in a wide variety of patients.

Ultrasonic transducers made with a single crystal offer noticeably better performance than those made from PZT, in terms of contrast and spatial resolution, uniformity from near field to far field (i.e., high signal-to-noise ratio), diagnostic confidence and accuracy; standard imaging, Doppler, colour flow and harmonic imaging performances are all enhanced. With these advantages, single crystals are highly desired for developing miniature transducers of superior performance (Zhou *et al.*, 2014).

On the negative side, single crystal transducers show higher electrical impedance, therefore difficult electrical matching with the system, and thinner piezoelectric layers than PZT. It is challenging to process single crystals designed for frequencies higher than 8 MHz because their thickness (< 200 μm) makes them fragile in this range. A major drawback in the production of single crystal transducers is the high cost due to lower yield and longer manufacturing time (Kim *et al.*, 2010; Ming Lu, Proulx, 2005). Another obstacle to the use of thin single crystals for high frequency transducers is the depoling phenomenon: if loss of polarization and sensitivity are to be avoided, a PMN-PT transducer must be driven by a voltage significantly lower than the typical system driving voltages (100 V or higher) (Ming Lu, Proulx, 2005).

Piezoelectric 1-3 and 2-2 composites are also commonly used in transducer technology. A piezoelectric 1-3 composite consists of piezoelectric rod-shaped pillars embedded in a passive epoxy matrix (Zhou *et al.*, 2014), whereas a composite 2-2 is made of alternating piezoelectric layer (such as PZT) and polymer layer (Fig. 5).

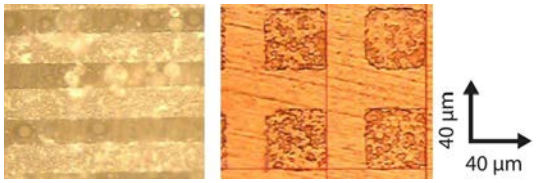

Fig. 5. Microscopic cross-sectional view of 2-2 composite (left) and 1-3 composite (right) ceramics. Note that the repeated structures shown here are smaller than a typical element within a transducer array of the type described below.

Piezoceramic/polymer composites have many advantages compared to monolithic ceramic: better acoustic impedance matching to the human body than PZT and single crystal (Table 2), low dielectric constant resulting in a high piezoelectric voltage constant, high coupling in the thickness mode for broad bandwidth, and ease of handling during transducer manufacture (Kwon *et al.*, 2003).

Table 2. Properties of PMN-PT single crystal, PZT and PZT-based 1-3 composite published by Kim *et al.* (2010).

Properties	PMN-PT single crystal	PZT-5A	PZT-based 1-3 composite
d_{33} [pC/N]	1780	374	593
k_{33}	0.92	0.71	0.75
Z [MRayl]	28.8	33.7	13.4

If two linear arrays at the same central frequency made with 2-2 CMP and PZT, respectively, are tested, the former one is expected to exhibit wider bandwidth but lower peak-to-peak amplitude of the pulse. The appropriate design solution depends on the given application. Ultrasonic arrays made with PZT-polymer composites are limited to frequencies < 30 MHz because of the difficulties in machining (sub-dicing) PZT ceramics to the tiny sizes necessary to create the PZT rods (Kwon *et al.*, 2003), although in a research context it has been shown that CMP manufacture by micromoulding is able to increase this limit to at least 100 MHz (Demore *et al.*, 2009a). Micro-moulding also allows the use of pillars that are neither cylindrical (rod-shaped) nor distributed in a regular pattern, both of which reduce the unwanted vibration modes that exist when there are few pillars per element (as is the case at high frequencies) (Demore *et al.*, 2009b).

A further increase in signal transmission efficiency is obtained using multi-layered crystal technology. The core of this architecture is a piezoelectric element composed of several layers (Hossack, Auld, 1993), which are mounted in the acoustic stack to improve electrical matching with the cable and reduce the energy and sensitivity loss due to the typical mismatch between the output impedance of the transducer and load impedance of the cable. As a result, image quality is enhanced. This technology encounters significant fabrication challenges as the layers must be electrically connected. Moreover, the bond thickness between the layers must be much smaller than the ultrasound wavelength, making the multi-layer crystal more suitable for mid-low frequency transducers. This technology requires a significantly complicated manufacturing process that increases the cost of good (Mills, Smith, 1999).

Another advance in ultrasound imaging consists of high-density arrays. They are characterized by finer-sized elements allowing enhanced compound, high frac-

tional bandwidth and reduced grating lobes, achieving increased contrast resolution, detailed resolution and high frame rate (Felix *et al.*, 2001; Hasegawa, de Korte, 1999). However, small elements can result in reduced manufacturing yield.

2.3. Micromachined ultrasonic transducers

Micromachined ultrasound transducers (MUTs) are a subset of MEMS (micro-electro-mechanical systems) structures that may substitute piezoelectric bulk ceramics for the design of transducers. A capacitive MUT (cMUT) consists of a membrane several tens of microns in diameter that is suspended a few tenths of micron above a silicon substrate (Savoia *et al.*, 2012; Dausch *et al.*, 2008; Khuri-Yakub, Oralkan, 2011). Connection electrodes are positioned on the membrane and substrate. In the presence of a bias voltage, the membrane is attracted to the substrate by the Coulomb force and restrained by elasticity of the membrane. If the electrostatic force exceeds the restoring force, the membrane collapses to the substrate; however, for an applied voltage just below collapse, the membrane is very sensitive to small changes in either applied voltage or displacement (i.e. transmitting or receiving US) (Wildes, Smith, 2012). Transducer elements are made by electrically connecting several cMUT membranes together. The main advantages of cMUTs are high spatial resolution from wide bandwidth (excess of 100%) and narrow elevational beam width due to easier manufacturability of multiple rows of elements (Dausch *et al.*, 2008) (see mention of 1.5D and 2D matrix arrays below), that are desired for visualising small structures, especially at high frequencies. On the negative side, electrical impedances tend to be higher than those for comparable piezoelectric devices. This leads to more complex circuitry to interface with the transmitter and receiver (Wildes, Smith, 2012). Another practical issue about cMUTs is that different designs are needed, depending on whether transmission or reception needs to be emphasised as the transmit transfer and receive transfer functions are different, whereas the transmitted and received responses of PZT based transducers are almost identical (Akasheh *et al.*, 2004; Warshavski *et al.*, 2016). cMUTs already form the basis of some commercial medical ultrasound probes.

Piezoelectric MUTs (pMUTs) are another approach, which work by taking advantage of the flexural motion of a thin membrane driven by a thin piezoelectric film (Abels *et al.*, 2017; Mastronardi *et al.*, 2014). Arrays of pMUTs are already exploited in fingerprint sensors and gesture detection and they are expected to be an ideal solution in the future for 3D/4D catheter-based imaging of the cardiovascular system. As yet, there are no pMUT-based commercial ultrasound probes as far as we know.

2.4. Multirow ultrasonic transducers

Most medical probes are 1D arrays consisting of a single row of transducer elements. The 1D arrays use electronic beamforming for beam steering and range-adjustable focusing in azimuth (Wildes, Smith, 2012), but rely on a fixed-range mechanical focus in the elevation direction. This means that the image slice thickness is non-uniform throughout the depth of the image and this affects the contrast resolution (Barthe, Slayton, 1996; Wildes, Smith, 2012). For instance, blood vessels or cysts are visible if the image slice thickness is comparable to or smaller than the vessel diameter, whereas they are averaged with the surrounding tissues and obscured if the slice thickness is much greater than the vessel size (Wildes, Smith, 2012). In other words, conventional 1D transducer arrays have good lateral and axial resolution, but elevation resolution is limited by the fixed-focus lens. Multi-row transducer arrays (Fig. 6) are used to provide a thin image slice over an extended depth of field, enhancing spatial and contrast resolution.

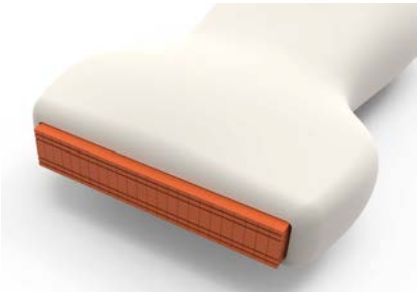

Fig. 6. Sketch of a multirow transducer: in this example, the array consists of 5 rows.

1.5D arrays have electronic multiplexing (switching) of elements and beamforming (relative delay adjustment between elements) in both azimuth and elevation, allowing dynamic control of the (still limited) elevation aperture and focus, while 1.25D arrays have only multiplexing (i.e., no relative delay adjustment between elements) allowing dynamic control of the elevation aperture but requiring static elevation focusing determined by a mechanical lens with a fixed focus (or foci) (Wildes, Smith, 2012). 2D matrix arrays, consisting of many thousands of transducer elements distributed in multiple rows, enable full electronic elevation apodization, focusing and steering. Such probes provide good resolution in the elevation direction due to their capability to focus US beams in two directions (elevation and azimuth) (Diarra *et al.*, 2012). Moreover they provide volumetric imaging in real time (Barthe, Slayton, 1996). The main disadvantage of the 2D array is the technological difficulty of connecting thousands of elements to the transmit and receive beamforming electronics, and the limited number of channels (typically a maximum of 256) availa-

ble in ultrasound systems due to the current high cost per channel of the electronics. These factors cause serious problems to the realization. Although the current solution in commercial scanners is to incorporate microbeamformers into the probe housing (Matrone *et al.*, 2014), multiplexing the beamformed signals back down so that such probes to be connected to a limited number (e.g., 256) of channels, this means that scanning of the sound beam still has to be employed for volumetric data acquisition, limiting the volume rate that can be achieved. For rapid real-time volumetric imaging, all probe elements must be connected simultaneously to scan the whole volume in the same beamforming operation (Diarra *et al.*, 2012) which is currently uneconomic. Many solutions are under investigation to provide a wide total aperture with high volume frame rate using a manageable number of active elements. For instance, this is the case of sparse 2D arrays that aim to limit the complexity for real-time 3D US applications, while optimizing the performance to ensure high quality volume images (Austeng, Holm, 2002; Diarra *et al.*, 2013; Lockwood, Foster, 1996; Ramalli *et al.*, 2015; Roux *et al.*, 2016; 2017).

3. US probe models and applications

US probes are available in a wide range of sizes, footprints, shapes and frequencies, specifically designed for particular clinical imaging applications and corresponding image format. The appropriate choice of probe depends on several factors, such as exam type, scan depth and patient characteristics. Probes may be classified into two main categories: conventional probes (linear, convex and phased arrays) and speciality probes that are dedicated to specific clinical applications (for instance, intraoperative and transesophageal probes) (De Luca *et al.*, 2018).

3.1. Conventional probes

The most prevalent US probe types are linear, convex and phased arrays (Fig. 7, Table 3).

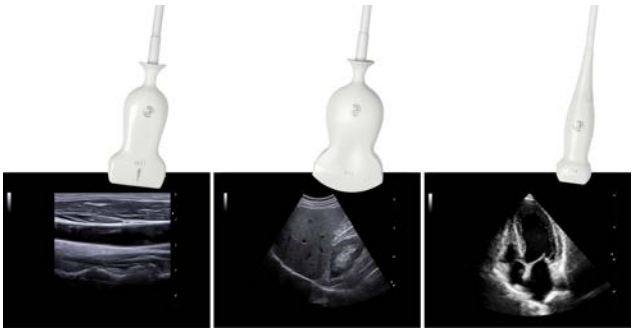

Fig. 7. Examples of conventional probes and their relative image formats (bottom): from left to right, linear, convex and phased arrays, showing carotid artery, liver and kidney, and heart respectively.

Linear Arrays (LAs) are flat and provide rectangular or trapezoidal image format with a depth-independent field of view that is roughly equal to the probe length (Wildes, Smith, 2012). They operate

Table 3. List of conventional probes including their operating range of frequency and intended use.

Probe type	Probe subtype	Typical frequency range [MHz]	Main clinical application sites
Phased	neonatal	4–13	cardiac, transcranial, abdomen
	pediatric	2–9	
	adult	1–5	cardiac, transcranial, abdomen, obstetrics (cardio-fetal)
Convex		1–8	abdomen (including vascular), gynecology, obstetrics
		2–9	small adult and pediatric abdomen (including vascular), obstetrics (1st and 2nd trimesters of pregnancy)
Microconvex		3–11	vascular, neonatal, pediatrics, transcranial
		1–7	abdomen, interventional
Linear	MF	3–11	vascular, pediatrics, superficial/small organs (e.g. breast, thyroid, testis), obstetrics
	HF	4–18	vascular, superficial/small organs, abdomen, musculoskeletal
	VHF	8–24	peripheral vascular, musculoskeletal, rheumatology, dermatology
	UHF	30–70	dermatology, pre-clinical research
Endocavity	end-fire	3–12	gynecology, obstetrics, urology
Transrectal	dual array linear/convex	4–13/3–13	urology
	dual array convex/convex	2–12/2–12	

over many frequency ranges, the choice of which depends on the tissue depth of interest (the higher the frequency, the better the resolution, but the poorer the depth of tissue penetration). LAs are typically used for superficial imaging of carotids, leg veins, thyroid, testicles, breast, musculoskeletal and vascular imaging (Szabó, Lewin, 2013). Breast imaging typically employs high frequency (HF) LAs that represent an invaluable diagnostic tool for measuring the size of tumors and inflammatory processes (Zhou *et al.*, 2014). Vasculature imaging remains at mid frequency (MF), in the range 3–11 MHz, due to the need to assess deeper leg veins and perform good Doppler examinations (Szabó, Lewin, 2013; Tortoli *et al.*, 1997; Wildes, Smith, 2012). In this frequency domain, the possibility of the array to add trapezoidal imaging format (extended field of view) is considered an advantage in obstetrics. Very high frequency (VHF) LAs, ranging between 8 MHz and 24 MHz, are typically dedicated to superficial musculoskeletal, rheumatology, dermatology and superficial vascular applications (Fig. 8). Ultra-high frequency (UHF, 30–70 MHz) LAs also exist for dermatology, for high resolution and noninvasive imaging of skin morphology and pathology. The information provided by these devices allows preoperative planning of margins for excision of skin tumours; in addition, skin thickness, skin echogenicity, burn scars, wound healing, skin aging and the nature of skin tumors can also be evaluated (Dinnes *et al.*, 2018; Zhou *et al.*, 2014). UHF US has also a significant potential for impact upon clinical imaging of eye diseases (Zhou *et al.*, 2014), even if in this case particular ophthalmic safety protection guidelines (ter Haar, 2011) have to be guaranteed by the scanner/probe, system.

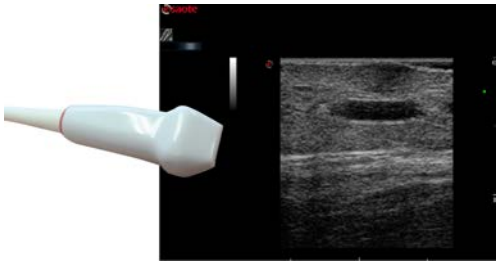

Fig. 8. VHF (22 MHz) linear array with small footprint, dedicated to rheumatology, dermatology, anaesthesiology, vascular, neonatal. As an example, a very superficial lipoma is shown: field of view 13 mm, depth of penetration 15 mm, focus at 2 mm.

Phased arrays (PAs) are also flat, but have smaller footprint to fit between ribs, being primarily used for cardiac imaging. The probe array size is on the order of 20×15 mm depending on manufacturer (Szabó, Lewin, 2013). To achieve a field of view sufficient to image the entire heart, the beam is steered to create a sector scan that has increasing field of view as a function of depth. The operating frequency depends on patient age, which affects depth of the heart: 4–13 MHz for neonatal, 2–9 MHz for pediatric, and 1–5 MHz for adult (Wildes, Smith, 2012). Pediatric probes also have smaller footprint than those used for adults, to cope with the smaller rib spacing. Transcranial probes are usually lower frequency (1–5 MHz) PAs, to image blood vessels within the skull using the temples as the US beam window (Szabó, Lewin, 2013). PAs may also be used for abdominal imaging, due to their small footprint and wide sector image format (Szabó, Lewin, 2013).

Convex linear arrays (CAs) are curved with a radius of curvature (ROC) in the range 40–60 mm. With a central frequency of roughly 3.5 MHz, they are typically used for 2D abdominal imaging applications, gynecology and obstetrics (Wildes, Smith, 2012). In recent years, CAs at higher frequency (1–9 MHz) have been used for obstetrics scanning during the first and part of the second trimester, and for the abdomen in so-called "easy" patients (body weight around 65 kg).

CAs with smaller ROC (13–20 mm), namely microconvex arrays, typically operate in the frequency range 3–11 MHz and are used for pediatrics, vascular and veterinary uses. Microconvex arrays specially designed for interventional use, mainly liver biopsy, have lower frequency (2–7 MHz). Endo-cavity arrays are also curved (ROC is typically 10–15 mm) and are placed at the end of the probe (end-fire arrays). They are designed to use the vagina for access in obstetrics and gynecology and the anus for imaging of prostate. More complex, are bi-plane transrectal probes that have dual arrays providing images in two orthogonal planes (Szabó, Lewin, 2013): linear + convex (4–13 MHz/3–13 MHz) or convex + convex (2–12 MHz/2–12 MHz) (Fig. 9).

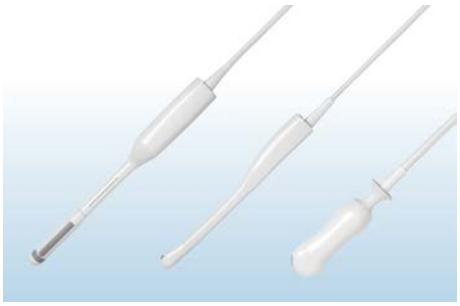

Fig. 9. From left to right, examples of bi-plane (linear + convex) transrectal, endocavity and microconvex probes.

Table 4 shows some ultrasonic probes specifically designed for dedicated applications, that are commonly used in the clinical routine.

Some ultrasonic transducers are specialized for imaging of internal organs from inside the body in a way that is more invasive than with endocavity probes. Transesophageal echocardiography (TEE) probes enable imaging of the heart from inside the

Table 4. Ultrasonic probes specifically designed for dedicated clinical applications, commonly used in the clinics.

Probe type	Features
Adult and pediatric trans-esophageal ecocardiography (TEE)	The transducer is attached to a thin tube that passes through the mouth, down the throat and into the esophagus, facilitating very clear imaging of the upper chambers and valves of the heart, being very close to these structures
Pencil Doppler	Non-imaging PW and CW Doppler for vascular, cardiac and transcranial Doppler evaluations
Hockey stick	Mainly dedicated to musculoskeletal and intraoperative imaging
Electro-mechanical 3D (LA, CA, endocavity, microconvex, LA with parallel acquisition)	Mechanically-swept arrays for 3D and 4D imaging
Matrix probe (LA, CA, PA, TEE)	Electronic 2D arrays for real-time volumetric acquisitions

esophagus (Fig. 10). As the esophagus is very close to the upper chambers and valves of the heart, TEE probes use higher frequency (≥ 5 MHz) and are implemented as phased arrays with manipulators and motors to adjust the orientation of the transducer (Szabó, Lewin, 2013). TEE 2D arrays enable electronic scanning for volumetric acquisition in real-time. To measure blood flow velocity, non-imaging US transducers, so-called CW and PW pencil transducers, may be used.

Fig. 10. Adult TEE phased arrays (left); Doppler colour flow mapping aids the diagnosis of a mitral valve insufficiency (right).

For volumetric image acquisition in real time, also known as 4D (3D acquisitions recorded over time) imaging (Fenster *et al.*, 2001; Nelson, Pretorius, 1998; Prager *et al.*, 2010; Provost *et al.*, 2014), either mechanically-swept 1D, 1.25D or 1.5D arrays, or electronic 2D arrays (Savord, Solomon, 2003), may be employed. Typically, mechanically-swept CAs are dedicated to abdominal, obstetrics (Fig. 11), gynaecology and contrast agent procedures, while mechanically-swept LAs are used in rheumatology, breast, small parts and vascular applications. Electronic 2D arrays are designed for real-time volumetric imaging in cardiology, women's health and vascular. Volumetric endoscopic probes also exist; they are particularly useful for differentiating adjacent tissues that have similar echogenicity, such as occurs when trying to discriminate ovaries, uterus and intestine adhesion in the presence of severe endometriosis.

Fig. 11. Mechanical-swept CA 3D probe and an example of volumetric acquisition in obstetrics.

3.2. Speciality probes

In intracardiac ecography (ICE), miniaturized phased arrays on the tip of a catheter have direct access to the inner chambers of the heart from within a vessel (Szabó, Lewin, 2013), while in intravascular ultrasound (IVUS) a catheter-tip VHF transducer allows imaging assessment of the morphological properties of the blood vessel wall (Szabó, 2004; Zhou *et al.*, 2014).

Surgical speciality probes include laparoscopic arrays, which are inserted through small incisions to image and aid in laparoscopic surgery, and intraoperative arrays specially designed to be used on vessels, organs and regions accessible during open surgery (Figs 12–14) (Szabó, Lewin, 2013).

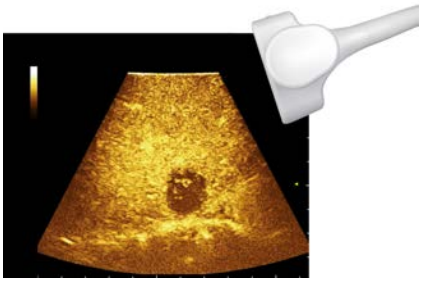

Fig. 12. T-shape linear array with ergonomic grip for intraoperative, abdominal, small parts, paediatric and vascular use, and an example of contrast enhanced ultrasound image of the liver (intraoperative view).

A more extensive (but still not exhaustive) list of speciality US probes currently available on the market, with a description of some of their features, is provided in Table 5.

Fig. 13. Dedicated convex array for 0°, 5°, 15° biopsy guidance for fine needle aspiration, biopsy or interventional procedures in abdominal, lung, urology. Liver biopsy example: the needle guidance overlaps the B-mode image.

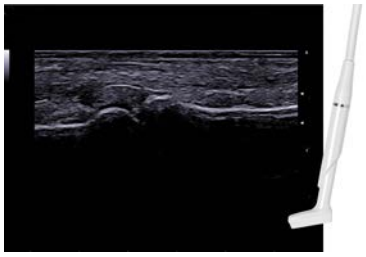

Fig. 14. Intraoperative hockey stick shaped linear array. As it works at high frequency (typically, in the range 6–18 MHz), it is also suitable for small parts, musculoskeletal, rheumatology, peripheral vascular. An example of finger US imaging is shown (right).

Table 5. List of speciality US transducers with a description of their notable features.

Speciality probe type	Features
TEE for long-term monitoring	Hemodynamic US for use in the intensive care unit
Transnasal micro-multiplane TEE	Micro TEE probe introduced trans-nasally to image, for example, the pituitary gland
Intracardiac echocardiography (ICE)	Imaging the heart from within the heart
Intravascular ultrasound (IVUS)	Imaging of blood vessel wall from within the vessel
Intraoperative bi-plane	Simultaneous biplane imaging with two orthogonal planes, providing greater control of needle placement
Laparoscopic	Imaging to guide and evaluate laparoscopic surgery
Fingertip probe	MC affixed on the sonographer's finger to maximize control for intraoperative, biopsy and vascular studies
Hockey stick with motorized tip	Intraoperative procedures
LA array manoeuvred by robotic surgery arm	Imaging to guide and evaluate laparoscopic surgery
3D Transrectal	Anorectal 3D imaging with 360°imaging field
Prostate Triplane	Images in 3 planes (transverse, sagittal, end-fire), plus 3D image reconstruction
Single probe with double transducer	Dual-headed probe integrating both LA and PA that allows for cardiac, vascular and abdominal applications. It is used in Emergency, POC, ICU.
Intraoral probe	Intra-oral structures imaging (sublingual gland, submandibular duct, tongue, lips, tonsils, soft palate)
Endoscopic US probe	It combines endoscopy and US to provide images of the organs inside the body such as stomach, esophagus, duodenum, lung and pancreas
USB probe	PA, LA and CA transducers with a simple USB connection
Wireless probe	Cable-free technology (CA, LA, PA)
Photoacoustic transducer	Photoacoustic imaging exploits the physical effect of the generation of acoustic waves by the absorption of optical energy. The probe includes optical elements for pulsed illumination of the tissue.
Veterinary probes	Dedicated probes for large animals, for example for imaging of the reproductive organs
Automated breast volume scanning (ABVS)	Mechanically-swept LA for user-independent and automated 3D near-whole breast imaging
3D whole breast US tomography	Circular, hemispherical or rotating linear array immersed in water for prone-patient and user-independent scanning with the use of sound that is transmitted through the organ as well as reflected by tissue structures within it.
Probes (CA, LA, PA) with programmable button on the handle	Dedicated probes specifically designed for easier single-operator biopsy and percutaneous procedures

3.3. Ergonomics

The percentage of sonographers reporting consequences of pain and discomfort is close to 80% within the first five years of entering the profession and 20% experience career-ending injuries (Andreoni *et al.*, 2015; Genovese, 2016; Gregory, 1998; Mazzola *et al.*, 2014b; 2017; Murphy, Russo, 2000). Manufacturers are constantly searching for housings designed to reduce work-related musculoskeletal disorders (WRMSDs) for sonographers. They are being made easy to handle and manipulate, lighter in weight, with rounded edges and smooth surfaces. Transducer cables are also becoming lighter in weight. A new probe design concept has been developed in recent years in order to reduce scanning fatigue and WRMSDs: transducers (appleprobe™ design) with a dual-possibility hand grip (pinch grip and palmar grip) are available in order to provide a neutral wrist position, reduced fatigue and easy handling (Fig. 15) (Mazzola *et al.*, 2014a; 2014b; 2017; Vannetti *et al.*, 2018).

Fig. 15. The palmar grip allowed by the appleprobe™ design (Esaote®), which enables a more neutral wrist position than that of the pinch grip.

3.4. Biopsy and virtual navigation

Biopsy kits for US probes are available for different uses and body areas, and for guidance of fine needle aspiration (FNA), percutaneous interventions and core biopsies (Fig. 16). Another accessory that can be attached to an US probe is a location and orientation sensor (usually electromagnetic or optical) for freehand 3D imaging and for virtual navigation (VN) systems that provide real-time fusion imaging (Fig. 17). In the most advanced solutions, either the biopsy kit or a single electromagnetic/optical sensor for VN, secured through a highly ergonomic mounting bracket on the probe, enable sufficient spatial accuracy and precision for the task and ensure a comfortable workflow which does not need probe-grip changes and does not generate a major probe-weight change (Andreoni *et al.*, 2015).

Fig. 16. Example of biopsy kit.

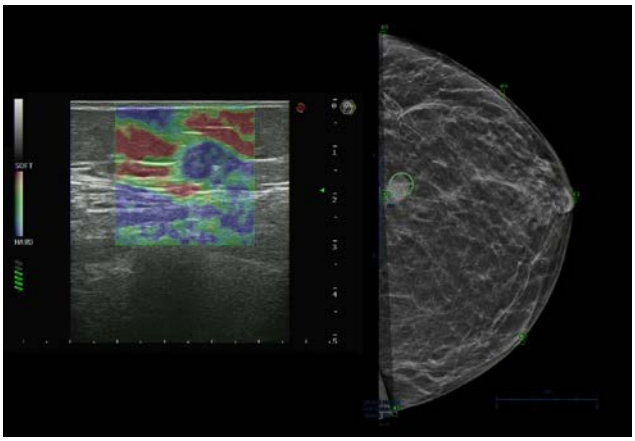

Fig. 17. 2D Navigation of the breast: on the left the elastogram is overlaid on the B-mode image, while on the right the relative mammogram is shown in real time for a more accurate diagnosis and localisation of the lesion. The green circle in the right image represents the US probe position that is placed in correspondence of the lesion.

4. Conclusion

The majority of ultrasonic probes currently available on the market has been described, together with technological insights that are responsible for image quality and a list of some of their clinical applications. Our aim was to provide information to healthcare professionals (including sonographers, physicians, biomedical/clinical engineers and other stakeholders involved in purchasing and maintaining medical devices) to select the appropriate probe for the intended use, taking account of the desired performance/price ratio. An overview of conventional and speciality probe types has been presented to summarize technical and clinical features, with the intention to satisfy information needed by the customer who uses ultrasound, which is a healthcare market segment that undergoes rapid innovations.

Acknowledgments

We thank Giovanni Altobelli, Michele Bassani, Guillaume Gauthier, Valentina Iorio, Marco Maglione (Esaote S.p.A.) for their kind and useful support in collecting all data summarized in this paper. JB acknowledges support from the EPSRC and Cancer Research UK.

References

1. Abels C. *et al.* (2017), Nitride-based materials for flexible MEMS tactile and flow sensors in robotics, *Sensors*, **17**(5): 1080, doi: 10.3390/s17051080.
2. Akasheh F., Myers T., Fraser J.D., Bose S., Bandyopadhyay A. (2004), Development of piezoelectric micromachined ultrasonic transducers, *Sensors and Actuators A: Physical*, **111**(2–3): 275–287, doi: 10.1016/j.sna.2003.11.022.
3. Andreoni G., Mazzola M., Matteoli S., D'Onofrio S., Forzoni L. (2015), Ultrasound system typologies, user interfaces and probes design: a review, *Procedia Manuf Elsevier*, **3**: 112–119, doi: 10.1016/j.promfg.2015.07.115.
4. Austeng A., Holm S. (2002), Sparse 2-D arrays for 3-D phased array imaging – Design methods, *IEEE Transactions on Ultrasonics, Ferroelectrics, and Frequency Control*, **49**(8): 1073–1086, doi: 10.1109/TUFFC.2002.1026019.
5. Azhari H. (2012), Ultrasound: medical imaging and beyond (an invited review), *Current Pharmaceutical Biotechnology*, **13**(11): 2104–2116, doi: 10.2174/138920112802502033.
6. Barthe P.G., Slayton M.H. (1996), 1.5-D ultrasound transducer array characterization, [in:] *Proceedings of 18th Annual International Conference of the IEEE Engineering in Medicine and Biology Society*, Vol. 2, pp. 895–897, doi: 10.1109/ULTSYM.1996.584355.
7. Chen Y.C., Wu S. (2002), Multiple acoustical matching layer design of ultrasonic transducer for medical application, *Japanese Journal of Applied Physics*, **41**(10R): 6098–6107.
8. Cho K., Baehyung K., Youngil K., Lee S., Jongkeun S. (2012), cMUT probe cooling design by thermal network, [in:] *2012 IEEE International Ultrasonics Symposium*, pp. 631–634, doi: 10.1109/ULTSYM.2012.0157.
9. Dausch D., Castellucci J., Chou D., von Ramm O. (2008), Theory and operation of 2-D array piezoelectric micromachined ultrasound transducers, *IEEE Transactions on Ultrasonics, Ferroelectrics, and Frequency Control*, **55**(11): 2484–2492, doi: 10.1109/TUFFC.956.
10. De Luca R., Dattoma T., Forzoni L., Bamber J., Palchetti P., Gubbini A. (2018), Diagnostic ultrasound probes: a typology and overview of technologies, *Current Directions in Biomedical Engineering*, **4**(1): 49–53, doi: 10.1515/cdbme-2018-0013.
11. Demore C.E.M. *et al.* (2009a), Functional characterisation of high frequency arrays based on micromoulded 1–3 piezocomposites, [in:] *2009 IEEE International Ultrasonics Symposium*, pp. 1134–1137, doi: 10.1109/ULTSYM.2009.5441966.
12. Demore C.E.M., Cochran S., Garcia-Gancedo L., Dauchy F., Button T.W., Bamber J.C. (2009b), 1–3 piezocomposite design optimised for high frequency kerfless transducer arrays, [in:] *2009 IEEE International Ultrasonics Symposium*, pp. 1–4, doi: 10.1109/ULTSYM.2009.5442007.
13. Diarra B., Liebgott H., Tortoli P., Cachard C. (2012), Sparse array techniques for 2Darray ultrasound imaging, *Acoustics 2012*, Nantes, France.
14. Diarra B., Robini M., Tortoli P., Cachard C., Liebgott H. (2013), Design of optimal 2-d nongrid sparse arrays for medical ultrasound, *IEEE Transactions on Biomedical Engineering*, **60**(11): 3093–3102, doi: 10.1109/TBME.2013.2267742.
15. Dinnes J. *et al.* (2018), High-frequency ultrasound for diagnosing skin cancer in adults, *Cochrane Database of Systematic Reviews*, **12**(12): CD013188, doi: 10.1002/14651858.CD013188.
16. Felix N., Ratsimandresy L., Dufait L. (2001), High bandwidth, high density arrays for advanced ultrasound imaging, [in:] *2001 IEEE Ultrasonics Symposium. Proceedings. An International Symposium* (Cat. No. 01CH37263), Atlanta, GA, USA, Vol. 2, pp. 1123–1126, doi: 10.1109/ULTSYM.2001.991916.
17. Fenster A. Downey D.B., Cardinal H.N. (2001), Three-dimensional ultrasound imaging, *Physics in medicine & biology*, **46**(5): R67–99, doi: 10.1088/0031-9155/46/5/201.
18. Genovese M. (2016), Ultrasound transducers, *Journal of Diagnostic Medical Sonography*, **32**(1): 48–53, doi: 10.1177/8756479315618207.
19. Gregory V. (1998), Musculoskeletal injuries: occupational health and safety issues in sonography, *Sound Effects*, http://citeseerx.ist.psu.edu/viewdoc/download?doi=10.1.1.463.6676&rep=rep1&type=pdf.
20. Hasegawa H., de Korte C.L. (2016), Impact of element pitch on synthetic aperture ultrasound imaging, *Journal of Medical Ultrasonics*, **43**(3): 317–325, doi: 10.1007/s10396-016-0700-6.
21. Hossack J.A., Auld B.A. (1993), Improving the characteristics of a transducer using multiple piezoelectric layers, *IEEE Transactions on Ultrasonics, Ferroelectrics, and Frequency Control*, **40**(2): 131–139, doi: 10.1109/58.212561.
22. Khuri-Yakub B.T., Oralkan O. (2011), Capacitive micromachined ultrasonic transducers for medical imaging and therapy, *Journal of micromechanics and microengineering*, **21**(5): 54004–54014, doi: 10.1088/0960-1317/21/5/054004.
23. Kim K.-B., Hsu D.K., Ahn B., Kim Y.-G., Barnard D.J. (2010) Fabrication and comparison of PMN-PT single crystal, PZT and PZT-based 1-3 composite ultrasonic transducers for NDE applications, *Ultrasonics*, **50**(8): 790–797, doi: 10.1016/j.ultras.2010.04.001.
24. Kochański W., Boeff M., Hashemiyan Z., Staszewski W.J., Verma P.K. (2015), Modelling and numerical simulations of in-air reverberation images for fault detection in medical ultrasonic transducers: a feasibility study, *Journal of Sensors*, **2015**: 1–14, doi: 10.1155/2015/796439.
25. Kwon S. *et al.* (2003), Ceramic/polymer 2-2 composites for high frequency transducers by tape casting, [in:] *IEEE Symposium on Ultrasonics*, Vol. 1, pp. 366–369, doi: 10.1109/ULTSYM.2003.1293424.

26. Lockwood G.R., Foster F.S. (1996), Optimizing the radiation pattern of sparse periodic two-dimensional arrays, *IEEE Transactions on Ultrasonics, Ferroelectrics, and Frequency Control*, **43**(1): 15–19, doi: 10.1109/58.484458.

27. Maione E., Tortoli P., Lypacewicz G., Nowicki A., Reid J.M. (1999), PSpice modelling of ultrasound transducers: comparison of software models to experiment, *IEEE Transactions on Ultrasonics, Ferroelectrics, and Frequency Control*, **46**(2): 399–406, doi: 10.1109/58.753029.

28. Mastronardi V.M., Guido F., Amato M., De Vittorio M., Petroni S. (2014), Piezoelectric ultrasonic transducer based on flexible AlN, *Microelectronic Engineering*, **121**: 59–63, doi: 10.1016/j.mee.2014.03.034.

29. Matrone G., Savoia A., Terenzi M., Caliano G., Quaglia F., Magenes G. (2014), A volumetric CMUT-based ultrasound imaging system simulator with integrated reception and μ-beamforming electronics models, *IEEE Transactions on Ultrasonics, Ferroelectrics, and Frequency Control*, **61**(5): 792–804, doi: 10.1109/TUFFC.2014.6805693.

30. Mazzola M., Forzoni L., D'Onofrio S., Andreoni G. (2017), Use of digital human model for ultrasound system design: a case study to minimize the risks of musculoskeletal disorders, *International Journal of Industrial Ergonomics*, **60**: 35–46, doi: 10.1016/j.ergon.2016.02.009.

31. Mazzola M., Forzoni L., D'Onofrio S., Marler T., Beck S. (2014a), Using Santos DHM to design the working environment for sonographers in order to minimize the risks of musculoskeletal disorders and to satisfy the clinical recommendations, *Proceedings of the 5th International Conference on Applied Human Factors and Ergonomics AHFE 2014*, Kraków, Poland, 19–23 July 2014.

32. Mazzola M., Forzoni L., D'Onofrio S., Standoli C.E., Andreoni G. (2014b), Evaluation of Professional Ultrasound Probes with Santos DHM. Handling comfort map generation and ergonomics assessment of different grasps, *Proceedings of the 5th International Conference on Applied Human Factors and Ergonomics AHFE 2014*, Kraków, Poland, 19–23 July 2014.

33. Mills D.M., Smith S.W. (1999), Multi-layered PZT/polymer composites to increase signal-to-noise ratio and resolution for medical ultrasound transducers, *IEEE Transactions on Ultrasonics, Ferroelectrics, and Frequency Control*, **46**(4): 961–971, doi: 10.1109/58.775663.

34. Ming Lu X., Proulx T.L. (2005), Single crystals vs. pzt ceramics for medical ultrasound applications, [in:] *IEEE Ultrasonics Symposium 2005*, pp. 227–230, doi: 10.1109/ULTSYM.2005.1602837.

35. Murphy C., Russo A. (2000), *An Update on Ergonomics Issue in Sonography, Burnaby, Employee Health and Safety Services at Healthcare Benefit Trust*, School of Kinesiology, Simon Fraser University, British Columbia, 2000.

36. Nelson T.R., Pretorius D.H. (1998), Three-dimensional ultrasound imaging, *Ultrasound in Medicine & Biology*, **24**(9): 1243–1270, doi: 10.1016/s0301-5629(98)00043-x.

37. Prager R.W., Ijaz U.Z., Gee A.H., Treece G.M. (2010), Three-dimensional ultrasound imaging, *Proceedings of the Institution of Mechanical Engineers, Part H: Journal of Engineering in Medicine*, **224**(2): 193–223, doi: 10.1243/09544119JEIM586.

38. Provost J. *et al.* (2014), 3D ultrafast ultrasound imaging in vivo, Physics in Medicine & Biology, **59**(19): L1–L13, doi: 10.1088/0031-9155/59/19/L1.

39. Ramalli A., Boni E., Savoia A.S., Tortoli P. (2015), Density-tapered spiral arrays for ultrasound 3-D imaging, *IEEE Transactions on Ultrasonics, Ferroelectrics, and Frequency Control*, **62**(8): 1580–1588, doi: 10.1109/TUFFC.2015.007035.

40. Roux E., Ramalli A., Liebgott H., Cachard C., Robini M.C., Tortoli P. (2017), Wideband 2-D array design optimization with fabrication constraints for 3-D US imaging, *IEEE Transactions on Ultrasonics, Ferroelectrics, and Frequency Control*, **64**(1): 108–125, doi: 10.1109/TUFFC.2016.2614776.

41. Roux E., Ramalli A., Tortoli P., Cachard C., Robini M.C., Liebgott H. (2016), 2-D ultrasound sparse arrays multidepth radiatio optimization using simulated annealing and spiral-array inspired energy functions, *IEEE Transactions on Ultrasonics, Ferroelectrics, and Frequency Control*, **63**(12): 2138–2149, doi: 10.1109/tuffc.2016.2602242.

42. Savoia A.S., Caliano G., Pappalardo M. (2012), A CMUT probe for medical ultrasonography: From microfabrication to system integration, *IEEE Transactions on Ultrasonics, Ferroelectrics, and Frequency Control*, **59**(6): 1127–1138, doi: 10.1109/tuffc.2012.2303.

43. Savord B., Solomon R. (2003), Fully sampled matrix transducer for real time 3D ultrasonic imaging, [in:] *Proceedings on IEEE Symposium on Ultrasonics, 2003*, Vol. 1, pp. 945–953, doi: 10.1109/ULTSYM.2003.1293556.

44. Spicci L. (2013), FEM simulation for "pulse-echo" performances of an ultrasound imaging linear probe, *COMSOL Conference*, Rotterdam, 2013.

45. Spicci L., Palchetti P., Gambineri F. (2017), *Ultrasound probe with optimized thermal management*, European patent EP3188664A1, European Patent Office.

46. Szabó T.L. (2004), *Diagnostic ultrasound imaging: inside out*, Elsevier, doi: 10.1016/C2011-0-07261-7.

47. Szabó T.L., Lewin P.A. (2013), Ultrasound transducer selection in clinical imaging practice, *Journal of Ultrasound in Medicine*, **32**: 573–582, doi: 10.7863/jum.2013.32.4.573.

48. ter Haar G. (2011), Ultrasonic imaging: safety considerations, *Interface Focus*, **1**(4): 686–697, doi: 10.1098/rsfs.2011.0029.

49. Tortoli P., Guidi G., Berti P., Guidi F., Righi D. (1997), An FFT-based flow profiler for high-resolution in vivo investigations, *Ultrasound in Medicine & Biology*, **23**(6): 899–910, doi: 10.1016/S0301-5629(97)00017-3.

50. Vannetti F., Atzori T., Fabbri L., Pasquini G., Forzoni L., Macchi C. (2018), Superficial electromyography, motion analysis and triggered-stereo cameras technologies applied to ultrasound system user interface evaluation, [in:] *Proceedings of the AHFE 2017 International Conferences on Human Factors and Ergonomics in Healthcare and Medical Devices*, July 17–21, 2017, Los Angeles, California, USA.

51. Warshavski O. *et al.* (2016), Experimental evaluation of cMUT and PZT transducers in receive only mode for photoacoustic imaging, [in:] *Proceedings of Photons Plus Ultrasound: Imaging and Sensing 2016*, Vol. 9708, doi: 10.1117/12.2211799.

52. Wildes D.G., Smith L.S. (2012), Advanced ultrasound probes for medical imaging, *AIP Conference Proceeding*, **1430**: 801–808, doi: 10.1063/1.4716307.

53. Yu Y.M., Chen M., Xiong Y., Chau M.M.C., Li R.S.H., Lau T.K. (2009), Comparison of conventional and PureWave crystal transducer in obstetric sonography, *The Journal of Maternal-Fetal & Neonatal Medicine*, **22**(7): 616–62, doi: 10.1080/14767050902801793.

54. Yue Q. *et al.* (2014), Fabrication of a PMN-PT single crystal-based transcranial Doppler transducer and the power regulation of its detection system, *Sensors*, **14**(12): 24462–24471, doi: 10.3390/s141224462.

55. Zhou Q., Lam K.H., Zheng H., Qiu W., Shung K.K. (2014), Piezoelectric single crystal ultrasonic transducers for biomedical applications, *Progress in Materials Science*, **66**: 87–111, doi: 10.1016/j.pmatsci.2014.06.001.